



Impact of PDO and AMO on interdecadal variability in extreme high temperatures in North China over the most recent 40-year period

Guwei Zhang¹ · Gang Zeng¹ · Chun Li² · Xiaoye Yang¹

Received: 26 August 2019 / Accepted: 31 January 2020
© Springer-Verlag GmbH Germany, part of Springer Nature 2020

Abstract

Based on the 1979–2018 datasets of Climate Prediction Center (CPC) daily maximum air temperature, HadISST, and NCEP-DOE II reanalysis, the impact of Pacific decadal oscillation (PDO) and Atlantic multidecadal oscillation (AMO) on the interdecadal variability in extreme high temperature (EHT) in North China (NC) is investigated through observational analysis and National Center for Atmospheric Research (NCAR) Community Atmosphere Model version 5.3 (CAM5.3) numerical simulations. The observational results show an interdecadal shift in NC's EHT in approximately 1996 with a cold period from 1983 to 1996 and a warm period from 1997 to 2014. The summer PDO and AMO are both closely related to NC's EHT, of which AMO dominates. From the cold to warm period, the combination of PDO and AMO changed from a positive PDO (+ PDO) phase and a negative AMO (– AMO) phase to a negative PDO (– PDO) phase and a positive AMO (+ AMO) phase. The shift in the antiphase combination of PDO and AMO plays an important role in the interdecadal transition of NC's EHT in 1996. PDO could impact NC's EHT through the Pacific-East Asia teleconnection pattern, and AMO could influence the NC's EHT through an atmospheric wave train in the midlatitudes of the Northern Hemisphere. During the warm period (– PDO and + AMO), warmer sea surface temperature anomalies (SSTA) in the northern North Pacific (NP) and North Atlantic (NA) could cause anticyclonic circulation anomalies over these two basins. The anticyclonic circulations anomalies over the NP could enhance the anticyclone over NC through the Pacific-East Asian (PEA) teleconnection pattern. It could also cause an easterly wind from the NP to NC which would weaken the upper westerly over NC. The anticyclonic anomalies over the NA, which were parts of the wave train, could affect other sectors of the wave train, resulting in anticyclonic anomalies over NC. The anticyclonic anomalies over NC could strengthen the continental high and weaken the upper zonal westerly, resulting in favorable EHT conditions. During the cold period (+ PDO and – AMO), because of the same atmospheric response mechanism, a westerly wind from NC to NP and a wave train with reversed anomaly centers could be found, causing a cyclonic anomaly over NC that is not conducive to the EHT. A series of numerical simulations using CAM5.3 confirm the above observational results and show that the combination of + PDO and – AMO changing to – PDO and + AMO has a great impact on the interdecadal shift in EHT in NC in 1996. The simulations also show that both + AMO and – PDO can lead the EHT in NC individually, and the impact of AMO on the EHT in NC is dominant.

Keywords Extreme high temperature · North China · Interdecadal variation · PDO · AMO · Numerical simulation

Electronic supplementary material The online version of this article (<https://doi.org/10.1007/s00382-020-05155-z>) contains supplementary material, which is available to authorized users.

✉ Gang Zeng
zenggang@nuist.edu.cn

¹ Key Laboratory of Meteorological Disaster of Ministry of Education (KLME), Collaborative Innovation Center on Forecast and Evaluation of Meteorological Disasters (CIC-FEMD), Nanjing University of Information Science and Technology, Nanjing 210044, China

² Physical Oceanography Laboratory and Key Laboratory of Ocean–Atmosphere Interaction and Climate in Universities of Shandong, Ocean University of China, Qingdao 266100, China

1 Introduction

Extreme high temperature (EHT) events have always been among the most important topics in meteorology because of the deep impacts on human lives and the social economy (McGregor et al. 2005). Under the background of global warming, EHT events occur more frequently in many regions around the world (Zhai et al. 1999; Meehl and Tebaldi 2004; Fischer and Knutti 2015). For example, Europe experienced record-breaking high temperatures in 2010 (Barrio et al. 2011), and the Yangtze River Delta region of China suffered from persistent high temperatures in the summer of 2013 (Sun 2014). Li and Sun (2017) indicated that the dominant teleconnection pattern over the Eurasian continent had a high impact on the interdecadal variability in EHT event frequency over the middle and lower reaches of the Yangtze River basin (MLYR). A positive teleconnection phase could weaken the upper westerly jet and upward movement of convergence over MLYR. In 2018, Northeast China suffered from an unusual summer EHT event with the maximum air temperature anomaly exceeding 6 °C (Tao and Zhang 2019). EHT has a serious impact on the lives and work of residents and leads to drought and crop yield reductions in many areas.

Located in the midlatitudes, North China (NC) is not only a political center but also a populated area and high-yield wheat region of China. In recent years, record-breaking high temperature events have occurred in many cities in NC. Regional high temperature events have become more frequent and enhanced in most regions of China, especially in NC (Wang et al. 2013). Xu et al. (2009) indicated that EHT events in NC exhibit an increasing trend. Ding et al. (2009) and Sun et al. (2011) both found that the number of EHT days in NC significantly increased after the mid-1990s. Deng et al. (2018) found that the concurrent variability in the heat waves in Eastern Europe and NC was mostly caused by an atmospheric circumglobal teleconnection with anticyclones over each region. An increasing number of researchers have begun to focus on the interdecadal variation of EHT events in NC (Sun et al. 2008; Yuan and Sun 2009; Cheng and Zhou 2014).

As important factors of global climate change, the Pacific decadal oscillation (PDO) and Atlantic multidecadal oscillation (AMO) have greatly impacted climate change in China (Wei et al. 2004; Yang and Li 2005; Lei et al. 2009; Han et al. 2017). Because AMO and PDO can modulate the atmospheric circulation system (Sun 2012; Zhu et al. 2013; Zhang and Delworth 2015), it is very important to study the effects of AMO and PDO on the EHT in NC. Deng et al. (2019) revealed that the unprecedented East Asian warming in spring 2018 is related to

the North Atlantic (NA) tripole sea surface temperature (SST) mode. Previous studies have noted that AMO is associated with thermohaline circulation (Delworth and Mann 2000; Zhang and Delworth 2005; Gulev et al. 2013; Delworth et al. 2016). The results of Lu et al. (2001) showed that the positive phase of AMO could lead to a strong East Asian Summer Monsoon (EASM). Li and Bates (2007) indicated that the positive AMO could warm the winters in most regions of China. Wang et al. (2009) thought that the positive AMO caused a rise in air temperatures in East Asia. Wu et al. (2016b) found that the second MV-EOF mode of the EASM was characterized by cyclonic anomalies over northeastern China and Japan, which was part of a circumglobal wave train. Furthermore, the researchers also found that the circumglobal teleconnection pattern was associated with forcing from AMO. Wang et al. (2017) found that the spring and summer AMO impacted the occurrence of the interdecadal Silk Road pattern (SRP) significantly, which has a key role in climate changes in China. Huang et al. (2018) indicated that an out-phase PDO and AMO could cause significant shifts in the East Asian jets. Some studies (Si and Ding 2016; Zhang et al. 2018) also found that PDO and AMO had great impacts on the interdecadal variability in the EASM precipitation. Zhu et al. (2016) investigated the combined impact of PDO and AMO on the summer monsoon in eastern China and found that the strongest signals occurred with an out-phase PDO and AMO. Zhang et al. (2018) indicated that when PDO and AMO were in different phases, the same SST anomalies occurred in the North Pacific (NP) and NA, and a zonal teleconnection wave train propagating from the NA to northern East Asia appeared across the mid-to-high latitudes of the Eurasian continent. Climate systems that affect precipitation can sometimes affect high temperature, and NC is in the region of the EASM. Thus, we consider that the summer PDO and AMO may impact the summer EHT in NC.

Has PDO and AMO influenced the EHT in NC in the most recent 40 years? How do PDO and AMO impact the EHT? And which one is dominant? This study will focus on these questions. The remainder of this paper is structured as follows. The data used in this study are described in Sect. 2. In Sect. 3, the methods used in this study are described and the interdecadal EHT characteristics in NC are demonstrated. In Sect. 4, the features of the atmospheric circulation anomalies in the warm and cold periods in NC are elaborated. In Sect. 5, the relationships between the EHT in NC and PDO and AMO are analyzed, and the effects of PDO and AMO on the interdecadal variations in the EHT are shown. Finally, the findings of this study are summarized and discussed in Sect. 6.

2 Data

Because of a good time correlation (0.98) and spatial similarity (Figure 1S) with the observational data in NC (CN05.1, Wu and Gao 2013), this study selected a global daily maximum temperature dataset provided by the Climate Prediction Center (CPC) to calculate the EHT indices from 1979 to 2018 (Xie and Arkin 1997). Its horizontal resolution is $0.5^\circ \times 0.5^\circ$.

The datasets used for analyzing atmospheric circulations include zonal and meridional winds, geopotential height and vertical p-velocity in pressure levels with a $2.5^\circ \times 2.5^\circ$ horizontal resolution from 1979 to 2018 provided by the National Centers for Environmental Prediction-Department of Energy (NCEP-DOE) Reanalysis II (Kanamitsu et al. 2002).

The monthly SST datasets from 1871 to 2018 are provided by the Hadley Centre (HadISST), with a horizontal resolution of $1.0^\circ \times 1.0^\circ$ (Rayner et al. 2003).

The PDO index is obtained from the University of Washington (<http://jisao.washington.edu/pdo/PDO.latest>). This index is defined as the leading standardized principal component of monthly SST anomalies in the NP, and more details can be found in Mantua et al. (1997) and Zhang et al. (1997). The AMO index is obtained from the National Center for Atmospheric Research (NCAR) (<http://www.cgd.ucar.edu/cas/catalog/climind/AMO.html>). This index is based upon the average anomalies of SST in the NA, typically over 0° – 80° N, and more details can be found in Trenberth and Shea (2006).

3 Methods

3.1 Statistics methods

In addition to a composite and correlation analysis (Zhu et al. 2013; Huang et al. 2018), liner regression (Kucharski et al. 2009), multiple regression analysis (Aiken and West 1991; Wang et al. 2017), Lanczos low-pass filtered method

(Duchon 1979) and the developed moving t test technique with effective freedom correction (Xiao and Li 2007) were used in this study. In order to eliminate the effects of global warming and better analyze the interdecadal variations, all datasets were removed linear trends firstly and then processed by low-pass filtering. The significance of the correlation is evaluated using the two-tailed Student's t -test, with the effective degree of freedom N_e , is calculated as follows:

$$N_e = N_o \frac{1 - r_1 r_2}{1 + r_1 r_2} \quad (1)$$

where N_o is the sample size; r_1 and r_2 are the lag-1 autocorrelation coefficients of the two series (Bretherton et al. 1999; Zhang et al. 2018; Miao et al. 2019; Napoli et al. 2019). It's also applied to evaluate the significance of linear correlation coefficients.

3.2 Heat indices

Three EHT indices were calculated in this study. They are warmest day (TXx), warm days (TX90p), and heat wave (HW), representing the intensity, frequency, and duration of EHT events, respectively (Table 1) (Meehl and Tebaldi 2004). To focus on the interdecadal variations, the data used were subjected to a 9-year low-pass filtering. The study season is summer (June–August), and the climatology definition is averaged from 1981 to 2010.

3.3 Location of North China

In this study, we define the domain (35° – 45° N, 110° – 120° E) as North China (Fig. 1a), which is similar to the definition of Cheng and Zhou (2014). The regional mean summer daily maximum surface air temperature (Tmax) anomalies and its 9-year moving average (black solid line) from 1979 to 2018 over North China exhibits a significant increasing trend and interdecadal variability (Fig. 1b). The moving t -test technique (Xiao and Li 2007) was employed to find the exact shift year, and its result shows that the shift year is 1996 (Fig. 1c). The three indices, i.e. TXx, TX90p and HW,

Table 1 Definitions of extreme heat indices

Acronym	Indicator	Definitions	Units
TXx	Warmest day	Maximum Tmax in summer	°C
TX90p	Warm days	Days when Tmax is larger than T90	days
HW	Heat wave	(1) The entire period must contain at least three consecutive days with a Tmax higher than T95 (2) the average Tmax of the entire period must be higher than T80; and (3) the Tmax of each day must be higher than T80	days

Where Tmax is the daily maximum surface air temperature. T95, T90 and T80 are 95%, 90% and 80%, respectively, of the local Tmax during 1979–2018

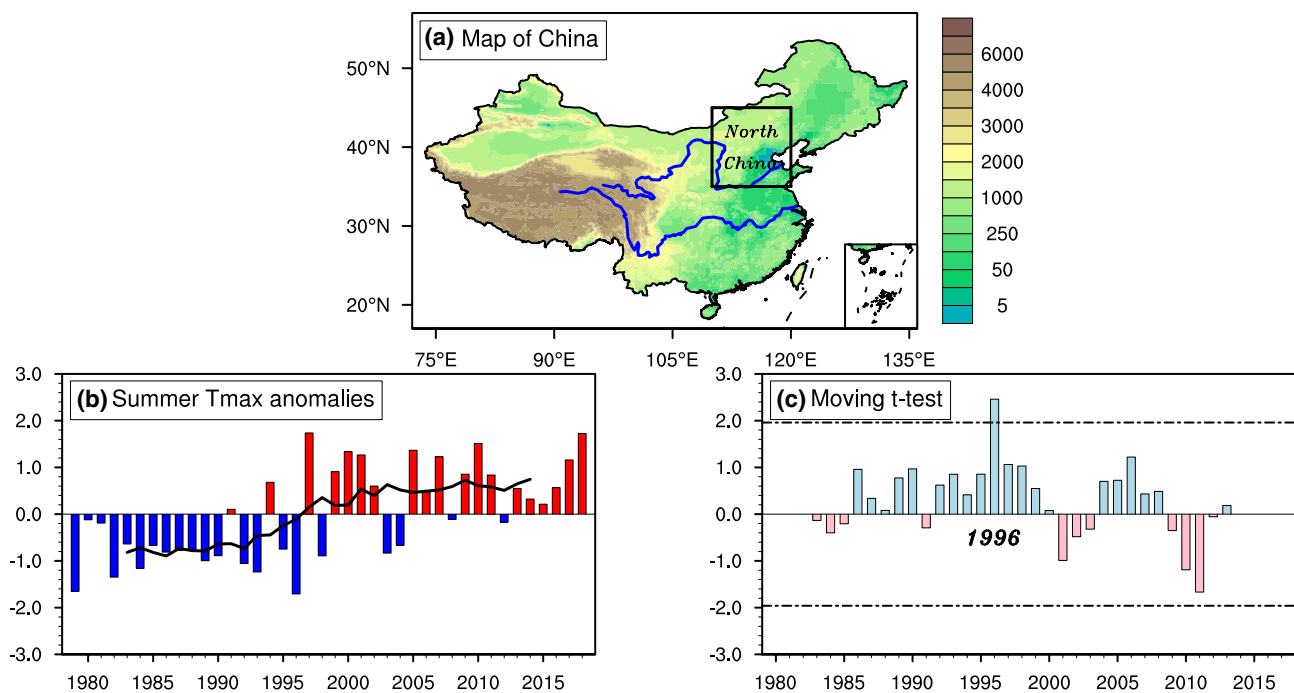


Fig. 1 **a** Map of China and the location of North China (black frame: 35°–45°N, 110°–120°E). The shaded denotes the terrain height (units: m). **b** Time series of regional mean HW anomalies in North China (filled bars) and its 9-year moving average (black solid line)

from 1979 to 2018. **c** The results calculated by developed moving t-test technique (filled bars). The black dotted lines in **(c)** represent significance at the 0.05 level

represent different features of EHT events, and they also show the same interdecadal variations (Figure S2). According to the results of the 9-year moving average (Fig. 1b), we finally choose the years from 1983 to 1996 as the cold period and the years from 1997 to 2014 as the warm period.

3.4 Numerical model

The Community Atmosphere Model version 5.3 (CAM5.3), as part of the Community Earth System Model version 1.2.2 (CESM1.2.2) modeling framework, is used in this study to investigate the possible physical mechanism of the interdecadal shift in summer EHT in North China. This model has been used in the previous studies of climate over East Asia (e.g. Zhang et al. 2016; Huang et al. 2018). The finite-volume dynamical core configured with a horizontal resolution of 1.9° latitude × 2.5° longitude (f19_f19) and 30 vertical hybrid levels is selected. More details about this model can be found in Neale (2012).

3.5 Wave activity flux

Wave activity flux (WAF) is used to determine the propagation of Rossby waves. The calculation of WAF is from Plumb (1985). Plumb (1985) used the conservation relationship of small amplitude steady wave propagation in a uniform zonal

flow and gave the three-dimensional WAF of the stationary Rossby wave to characterize the wave energy and propagation direction. The WAF formula is as follows:

$$F_s = \frac{p}{p_0} \cos \varphi \times \begin{pmatrix} v'^2 - \frac{1}{2\Omega \sin 2\varphi} \frac{\partial(v'\Phi')}{\partial \lambda} \\ -u'v' + \frac{1}{2\Omega \sin 2\varphi} \frac{\partial(u'\Phi')}{\partial \lambda} \\ \frac{f}{s} \left[v'T' - \frac{1}{2\Omega \sin 2\varphi} \frac{\partial(T'\Phi')}{\partial \lambda} \right] \end{pmatrix} \quad (2)$$

where variables marked with a superscript of “'” or “'” represent zonal mean and zonal deviation, respectively. (φ, λ) represents latitude and longitude, and (a, Ω) is the radius of the Earth and the Earth’s rotation rate. $f = 2\Omega \sin \varphi$ represents the Coriolis parameter, and (Φ, T) indicates the potential height and temperature. Static stability is presented by s , which is expressed as follows:

$$s = \frac{\partial \bar{T}}{\partial z} + \frac{\kappa \bar{T}}{H} \quad (3)$$

where $\kappa \approx 0.286$ is the ratio of gas to specific heat at constant pressure. $H = 8$ km is the constant height.

4 Atmospheric circulation anomalies

During the cold period, NC is occupied by negative geopotential height anomalies at 500 hPa with a central value exceeding -0.4 dagpm (Fig. 2a). The situation during the warm period is the opposite (Fig. 2b): NC is controlled by positive geopotential height anomalies at 500 hPa with a central value exceeding 0.6 dagpm. This indicates that the warm period in NC was controlled by the enhanced warm continental high pressure, which was conducive to the solar radiation reaching the surface and thus to the EHT events.

Previous studies have concluded that the upper zonal westerly is closely related to changes in vertical movements and clouds, while the changes could affect radiation, precipitation, and so on, which could eventually lead to temperature change (Liang and Wang 1998; Lu et al. 2001; Gong and Ho 2003; Sun 2014). The anomalies in the horizontal wind in the upper troposphere (300 hPa) during the cold period and warm period are shown in Fig. 2c, d, respectively. Easterly anomalies are found in the warm period, while westerly anomalies are found in the cold period. This finding indicates that the upper zonal westerly wind is weakened during the warm period and enhanced during the cold period. As shown in Fig. 3, the Tmax together with the three EHT

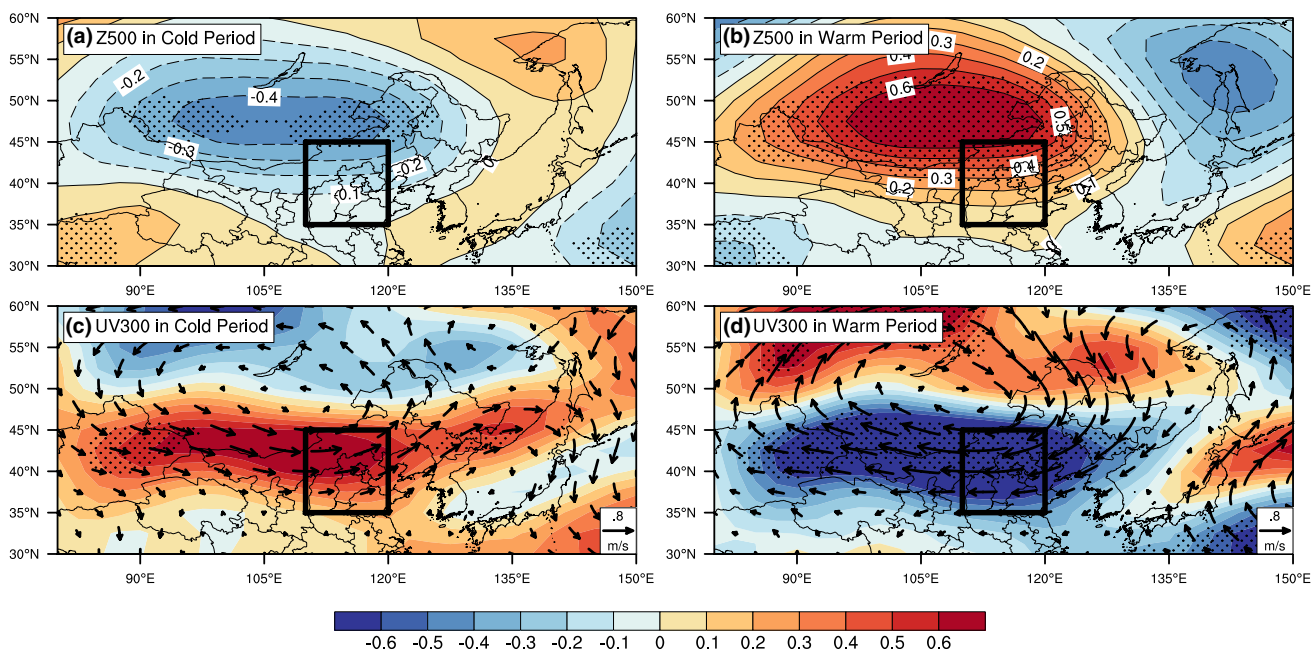


Fig. 2 Geopotential height anomalies at 500 hPa (shaded, dagpm) in the cold period (a) and warm period (b). Wind anomalies at 300 hPa (vector, m/s; shaded is horizontal velocity) in the cold period (c) and

warm period (d). The black frame in each figure shows the location of North China. Dotted areas denote statistical significance at the 0.05 level according to the Student's *t*-test

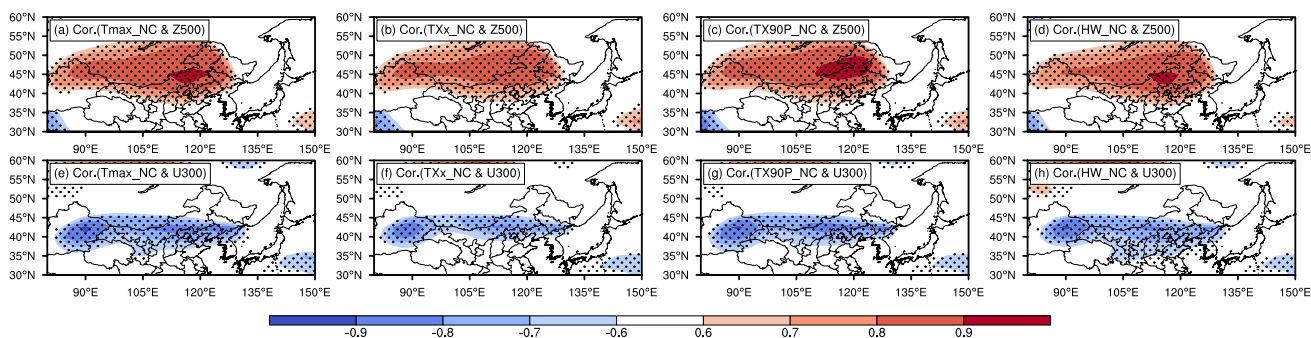


Fig. 3 Correlation coefficient pattern of the Z500/U300 with North China's summer Tmax (a)/(e), TXx (b)/(f), TX90p (c)/(g) and HW (d)/(h) during 1979–2018 (shaded). Dotted areas indicate statistical significance at the 0.05 level according to the Student's *t*-test

indices show a positive correlation with the geopotential height at 500 hPa (Z500) and a negative correlation with the zonal wind at 300 hPa (U300) over NC. This means that when the Z500 and U300 over NC, namely, the continental high and upper zonal westerly, increase (decrease) and decrease (increase), respectively, NC will become warm (cold).

Therefore, it is considered in this study that the continental high and the upper zonal westerly over NC are the main atmospheric circulation factors affecting the EHT.

5 Impacts of PDO and AMO

5.1 Observational results

Summer sea surface temperature anomalies (SSTA) in the NP and NA during the two periods are shown in Fig. 4a, b. It is easy to find a pattern such as the negative PDO (− PDO) and a pattern such as the positive AMO (+ AMO) in the warm period (Fig. 4b) and patterns such as the positive PDO (+ PDO) and the negative AMO (− AMO) in the cold period. The time series of summer PDO (Fig. 4c) and AMO (Fig. 4d) from 1979 to 2018 have similar interdecadal variations with the EHT in NC, that is, in the mid-to-late 1990s, the PDO phase changed from positive to negative, and the AMO phase changed from negative to positive. We also find that in the cold (heat) period, PDO and AMO are in a positive (negative) and negative (positive) phase,

respectively. The average values of PDO and AMO during the cold (warm) period are 0.94 (− 0.26) and − 0.07 (0.25). Thus, the cold period is considered to be the combination of + PDO and − AMO, while the warm period is considered to be the combination of − PDO and + AMO.

As shown in Fig. 5, the Tmax together with three EHT indices (TXx, TX90p and HW) show good correlations with the summer SST in the NP (Fig. 5a–d) and NA (Fig. 5e, f). The significant correlation patterns also have similar SST distributions: the positive (negative) significant correlations are in the northern (southern) part of the NP, and the positive significant correlations are in most areas of the NA. Significant positive correlations occur both at decadal and interannual time scales between the summer AMO and each EHT index in NC. The summer PDO has significant negative correlations with Tmax and TXx (TX90p) at decadal (interannual) time scale (Table 2). It is obvious that both of them have contributions to the 1996's interdecadal shift of EHT in NC.

Therefore, we speculate that the configuration of PDO and AMO is closely related to the EHT events in NC during 1979–2018. The combination of + PDO and − AMO changing to − PDO and + AMO may be the main reason for the interdecadal shift in North China's EHT in approximately 1996

The decadal and interannual correlation coefficients between PDO and AMO are both significantly negative (− 0.54 and − 0.31). The impacts of PDO and AMO on NC could be individual and combined. Because NP is

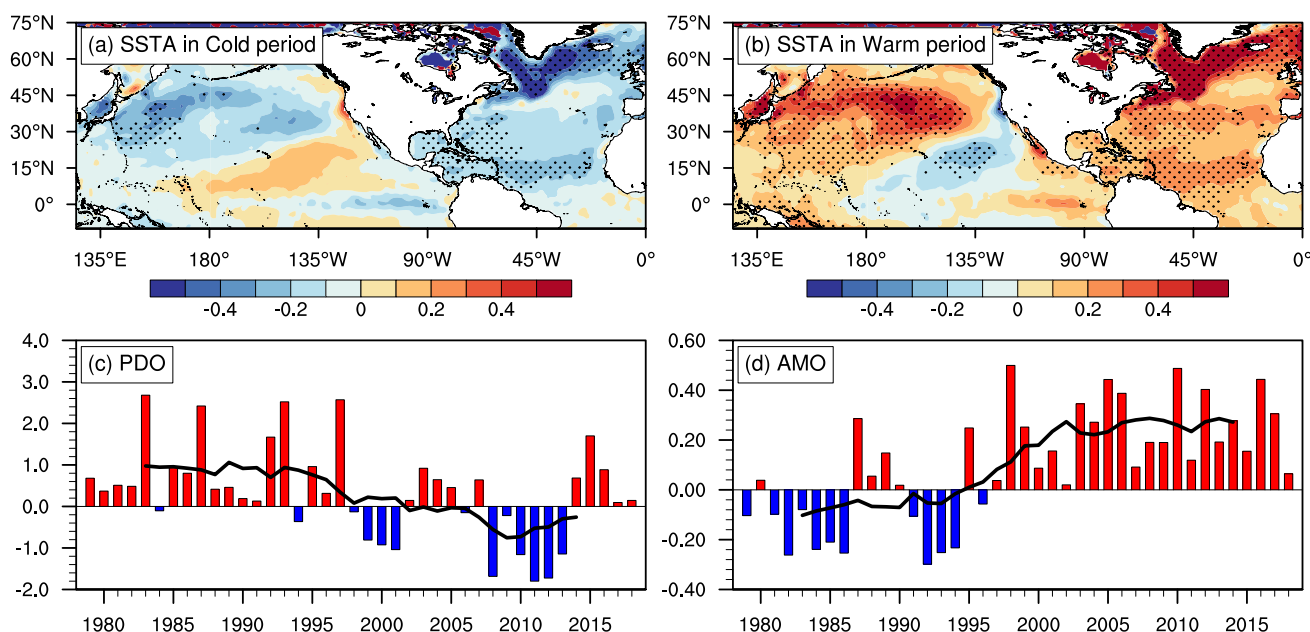


Fig. 4 The SST anomalies in the **a** cold period and **b** warm period (°C). The time series (filled bars) of summer **c** PDO and **d** AMO from 1979 to 2018 with their 9-year moving average (black solid

line). Dotted areas are statistically significant at the 0.05 level according to the Student's *t*-test

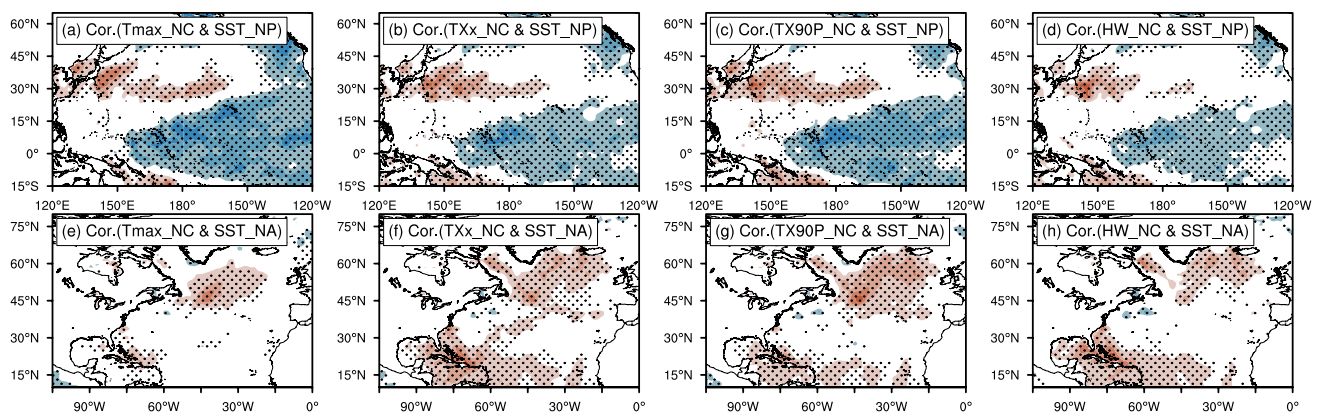


Fig. 5 Correlation coefficient pattern of the SST in the NP with North China's summer **a** Tmax, **b** TXx, **c** TX90p and **d** HW during 1979–2018 (shaded). The correlation coefficient pattern of the SST in the

NA against North China's summer **e** Tmax, **f** TXx, **g** TX90p and **h** HW during 1979–2018 (shaded). Dotted areas denote statistical significance at the 0.05 level according to the Student's *t*-test

Table 2 Decadal (interannual) correlation coefficients between PDO/AMO and North China's summer EHT indices

	PDO	AMO	Tmax	TXx	TX90p	HW
PDO	–	– 0.54 (– 0.31)	– 0.57 (– 0.33)	– 0.53 (– 0.21)	– 0.51 (– 0.30)	– 0.50 (– 0.18)
AMO	– 0.54 (– 0.31)	–	0.72 (0.40)	0.80 (0.49)	0.85 (0.41)	0.71 (0.35)

Correlation coefficients in bold are significant at the 0.05 level

located close to NC, the most impacts of PDO on NC is probably local or basin scale. Wang et al. (2019) found that the – PDO could impact the severity of the autumn drought in NC through the Pacific-East Asian (PEA) teleconnection pattern. In this study, we consider the mechanism of the PDO in summer is similar. Figure 6c, d shows that there are anticyclone-cyclone-anticyclone/cyclone-anticyclone-cyclone (ACA/CAC) circulation anomalies in the upper level from the NP to NC in the warm/cold period. During the warm period (– PDO), the anticyclonic circulation anomalies caused by the warm SSTA (Fig. 4b) in the northern NP (NNP) could enhance the anticyclonic anomalies over NC through the PEA. The enhanced anticyclonic circulation over NC could lead to the local downward motion (Fig. 6b), which is conducive to getting warm. In addition, there is a counter-clockwise vertical circulation anomalies located from NC (110–20°E) to the Sea of Japan (~ 135°E) in Fig. 6b. The easterly wind anomalies in the high level of this vertical circulation can weaken the upper zonal westerly over NC. While in the cold period (+ PDO), the SSTA in the NNP is cold (Fig. 4a). The mechanism is the verse: the cyclone circulations over the NNP enhance the cyclonic anomalies over NC through the PEA (Fig. 6c), which would lead the upward motion and not conducive to rising temperature (Fig. 6a); the local vertical circulation from NC to the Sea of Japan is clockwise, which means the westerly wind

anomalies are in the high level; the westerly winds could enhance the upper zonal westerly over NC (Fig. 6a).

Zhang et al. (2018) concluded that changes in SSTA in the NP and NA could affect the climate of East Asia by teleconnection. Our study also studied the combined impacts of the PDO and AMO on NC's EHT. As shown in Fig. 7, the partial correlation coefficient patterns of summer PDO and AMO with meridional wind at 300 hPa (V300) during 1979–2018 both seem like a wave train in the midlatitudes of the Northern Hemisphere. The V300 anomalies in the cold period (Fig. 8a) and warm period (Fig. 8b) both show a significant cyclonic-anticyclonic teleconnection wave train in the midlatitudes of the Northern Hemisphere. The wave trains resemble the interdecadal circumglobal teleconnection pattern in Wu et al. (2016a). The part of the wave trains over NA and Europe were similar to the North-Atlantic-European East West (NEW) mode found by Ghosh et al. (2017), and the sector over Eurasia is similar to the interdecadal SRP (Wang et al. 2017). The wave train in our study is opposing patterns in the warm and cold periods. In the warm/cold period (Fig. 8a, b), the circulation anomalies over NA, NP and NC are anticyclonic/cyclonic, and they are parts of the wave trains. In the warm (cold) period, significant positive (negative) anomalies of Z300 over the NA, NC and the NP demonstrate a kind of atmospheric circulation that is conducive (not conducive) to NC's EHT (Fig. 9a, b). The eastward WAF indicates that

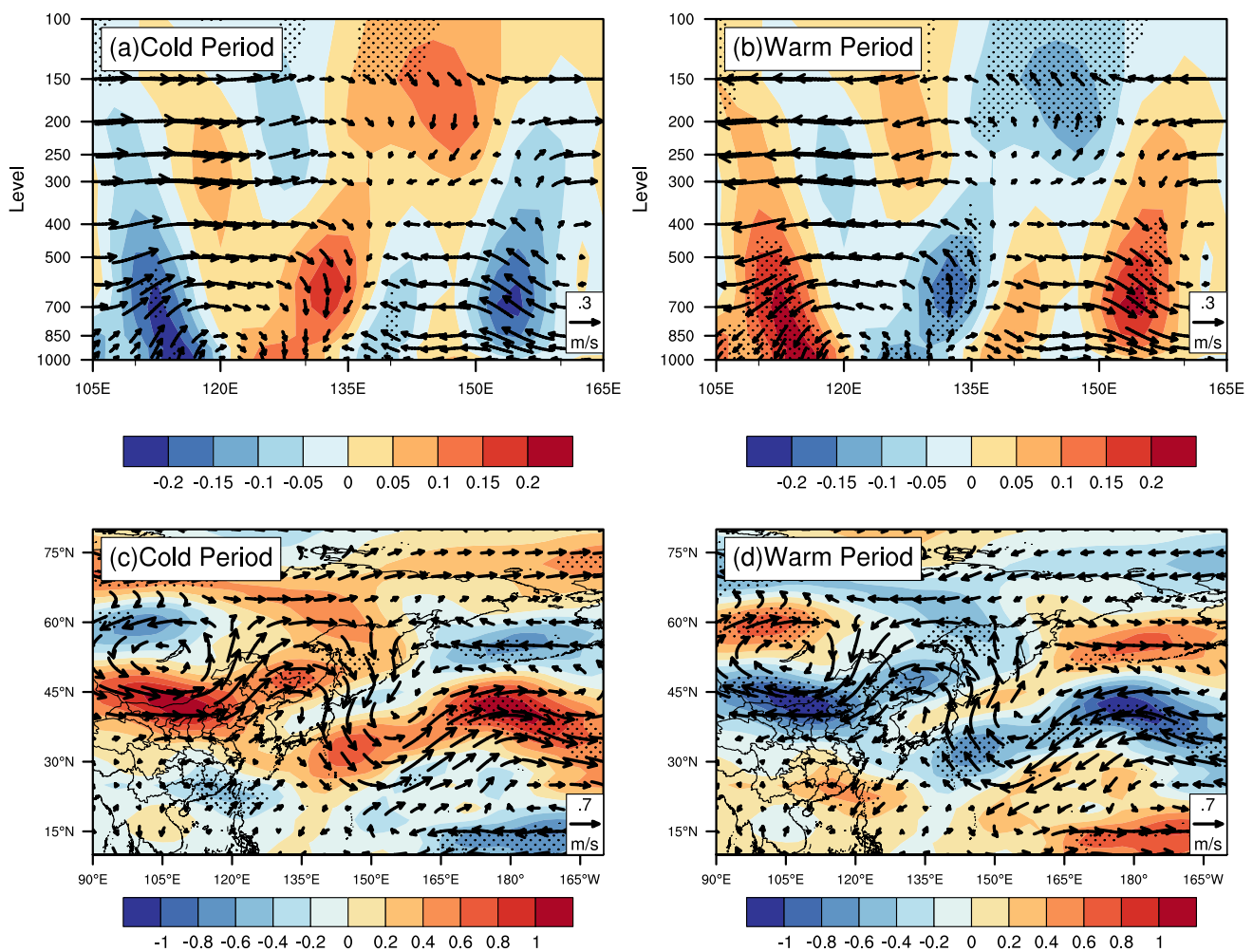


Fig. 6 **a/b** Longitude–pressure sections of vertical circulation anomalies averaged from 35 to 45°N (vector, units of vertical and zonal wind are 10^{-2} Pa/S and m/s, respectively; shaded is vertical velocity) and **c/d** horizontal wind anomalies (vector, m/s, shaded is meridi-

onal velocity) at 200 hPa during the cold period/warm period. Dotted areas denote statistical significance at the 0.05 level according to the Student's *t*-test

this wave train propagates from the NA to the NP along the Eurasian continent in the midlatitudes. The significant partial correlation patterns in NC only show in the results of AMO (Fig. 7b), not in the PDO (Fig. 7a). This means that although PDO could affect the wave train, the impacts of PDO through the wave train on NC may be less. Ghosh et al. (2017) noted that the NEW mode is associated with the AMO. Wang et al. (2017) proposed that the AMO signals were captured by the subtropical and subpolar jet streams, formed the SRP and influenced the climate over NC. Thus, the wave train in the warm/cold period may be caused by the + AMO/– AMO. + AMO/– AMO may cause significant positive/negative Z300 and anticyclonic/cyclonic circulations over NA through air–sea interactions, thereby affecting the wave train. The multiple linear regression of EHT in NC by AMO and PDO indicate that their standardized regression coefficients are statistically

significant, 0.61 for AMO and -0.23 for PDO. Therefore, PDO and AMO both have contributions to the 1996's shift of NC's EHT, but the impacts of AMO is dominant.

In summary, PDO and AMO can influence the EHT in NC through the PEA and the wave train, respectively. The anticyclonic circulations over the NP can enhance the anticyclonic anomalies over NC via PEA, and the easterly wind of the local vertical circulation from NC to the Sea of Japan can weaken the zonal upper westerly over NC. The anticyclones over the NA can affect the wave train and strengthen anticyclonic anomalies over NC, resulting in EHT events. In the cold period (+ PDO and – AMO), due to the same atmospheric response mechanism, a wave train with reversed anomaly centers compared with the warm period and a westerly wind from NC to the Sea of Japan can both be found in the midlatitudes of the Northern Hemisphere.

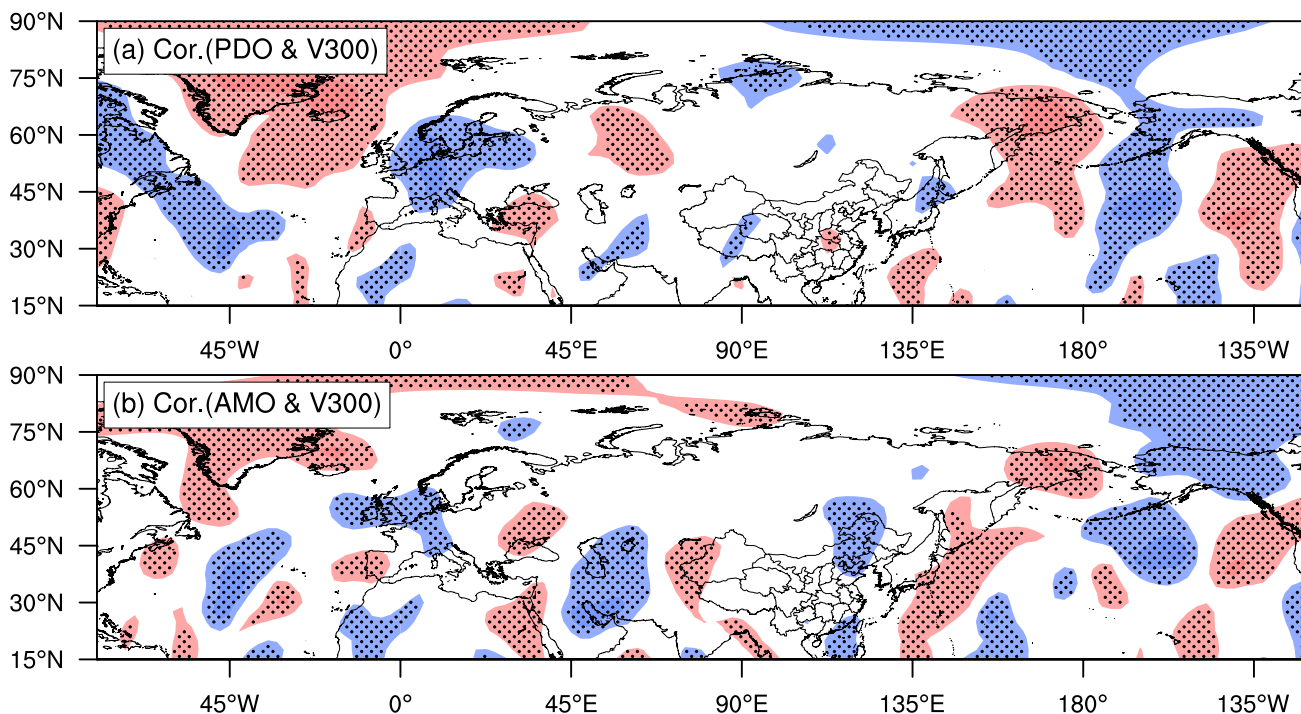


Fig. 7 Partial correlation coefficient patterns of summer **a** PDO and **b** AMO with meridional wind at 300 hPa (V300) during 1979–2018 (shaded). Red (blue) shaded areas indicate positive (negative) value.

Dotted areas denote statistical significance at the 0.05 level according to the Student's *t*-test

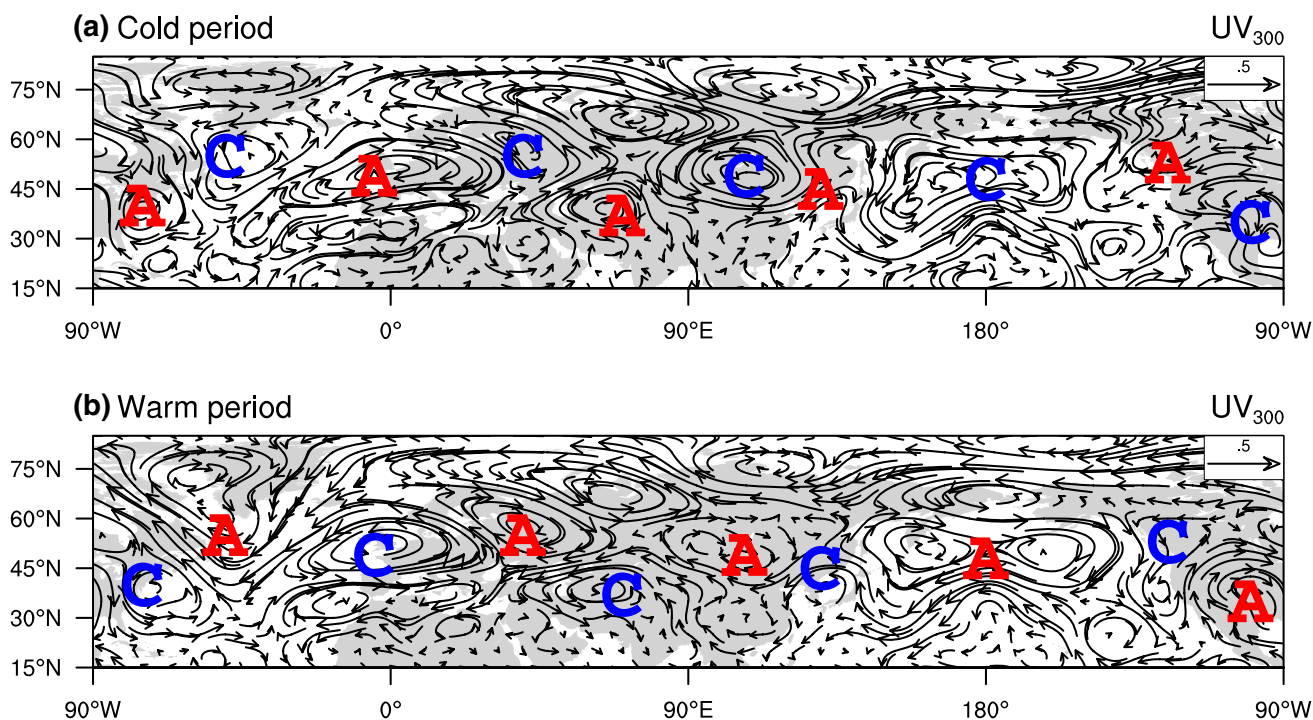


Fig. 8 Horizontal wind anomalies (vector, m/s) at 300 hPa during the cold period **a** and warm period **(b)**. Red “A” and blue “C” represent anticyclonic and cyclonic circulations, respectively

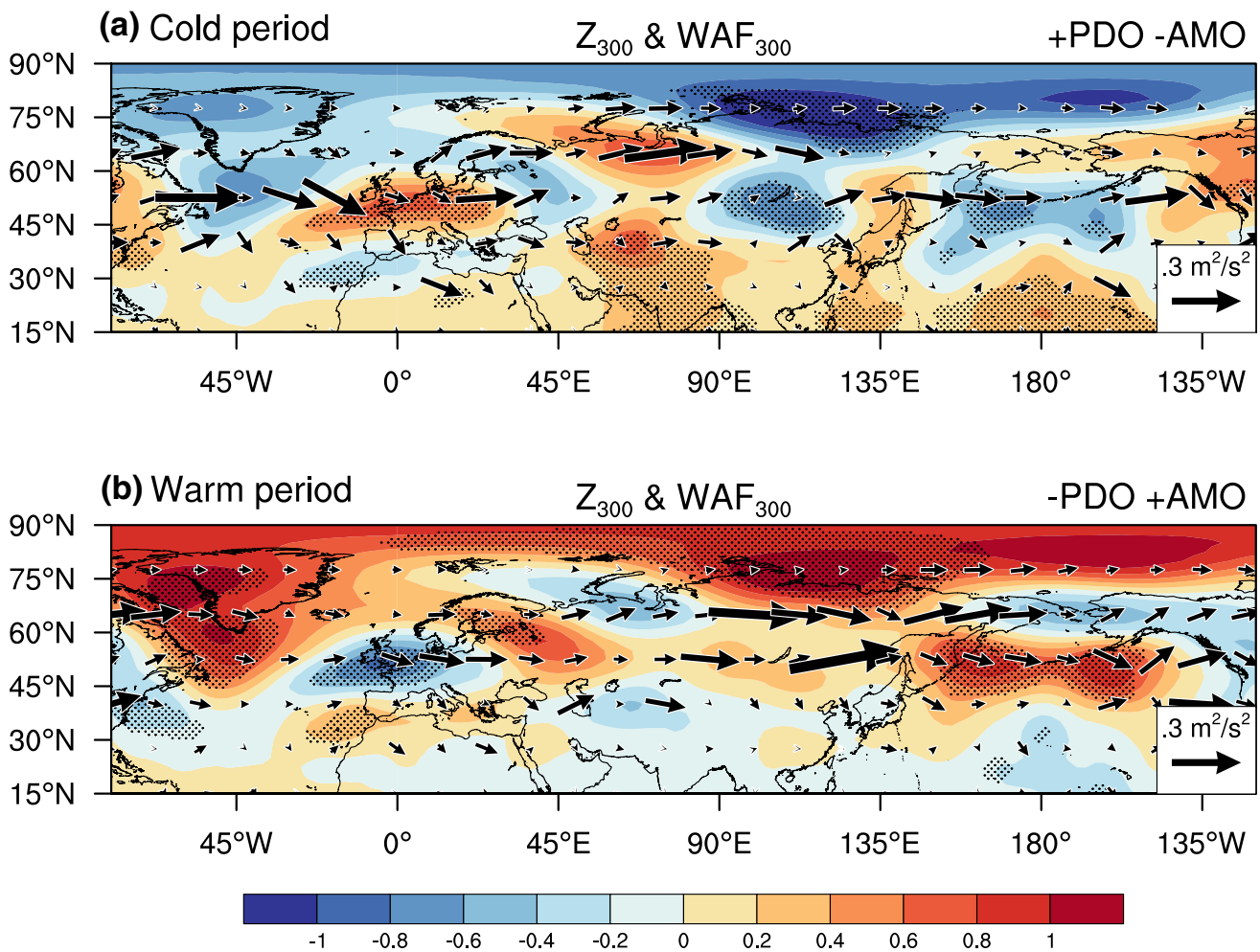


Fig. 9 Geopotential height anomalies (shading, dagpm) and WAF (vector, $m^2 \cdot s^{-2}$) at 300 hPa during the cold period (a) and warm period (b). Dotted areas denote statistical significance at the 0.05 level according to the Student's *t*-test

Table 3 Descriptions of one control experiment and six sensitivity experiments using the CAM5.3 atmospheric model

Experiments	Members	Years	Description
CTRL	50	5	Forced by climatological SSTs.
PpAn	50	5	In each summer, the SSTs in regions A and B are the summer +PDO and -AMO period ensemble means, respectively, while other regions are climatological SSTs. In other seasons, the global are climatological SSTs
PnAp	50	5	Same as the PpAn but the summer SSTs in regions A/B are summer -PDO/+AMO period ensemble means
Pp	50	5	In each summer, the SSTs in region A are the summer +PDO period ensemble means, while other regions are climatological SSTs. In other seasons, the global are climatological SSTs
Pn	50	5	Same as the Pp but the summer SSTs in region A are the summer -PDO period ensemble means
Ap	50	5	In each summer, the SSTs in region B are the summer +AMO period ensemble means, while other regions are climatological SSTs. In other seasons, the global are climatological SSTs
An	50	5	Same as the Ap but the summer SSTs in region B are the summer -AMO period ensemble means

5.2 Numerical experimental results

Based on the above observational analysis, the main possible causes of the EHT event interdecadal increase in NC can be summarized as follows: the enhanced continental high and weakened zonal westerly wind are mainly caused by summer $-$ PDO and $+$ AMO through the PEA and the cyclonic-anticyclonic teleconnection wave train in the midlatitudes of the Northern Hemisphere. To prove the findings of the observational results, several numerical experiments (Table 3) with CAM5.3 are conducted for analysis. We considered the PDO region (20° – 65° N, 120° E– 120° W) to be region A and the AMO region (0° – 65° N, 80° W– 0°) to be region B, and then defined the cold/warm periods (1983–1996/1997–2014) as the periods of \pm PDO and \mp AMO.

Descriptions of the seven numerical experiments are shown in Table 3. Each experiment contains 50 members, and each member run of 5 years is forced by different initial conditions. The ensemble simulations are considered to be the analytical data of each experiment. The model is forced by climatological SSTs in the control experiment (CTRL). The six sensitivity experiments are mostly the same as the CTRL but are performed separately for different phases of the summer PDO and AMO. The PpAn/PnAp experiment represents the summer \pm PDO together with the summer \mp AMO, which is with imposed summer \pm PDO period ensemble mean SSTs in region A and summer \mp AMO period ensemble mean SSTs in region B. These two experiments are used to study the impacts of the combination of \mp PDO

and \pm AMO on EHT events in NC. The Pp/Pn experiment represents the summer \pm PDO which is with imposed summer \pm PDO period ensemble mean SSTs in region A. The Ap/An experiment represents the summer \pm AMO which is with imposed summer \pm AMO period ensemble mean SSTs in region B. These four experiments are used to study the individual impacts of PDO and AMO on EHT events in NC. The SSTA distributions of each sensitivity experiment, which are the results of the input SST in each sensitive experiment minus the SST in CTRL, are shown in Fig. 10.

The summer Tmax anomalies in NC of PpAn (Fig. 11a) and PnAp (Fig. 11b) are negative and positive, respectively. This finding is consistent with the observations and proves that the combination of $-$ PDO and $+$ AMO can cause the warmer NC. The geopotential height anomalies at 500 hPa for PpAn (Fig. 11c) and PnAp (Fig. 11d) also showed a weakened and enhanced continental high over NC, which means that the combination of $-$ PDO and $+$ AMO could result in conditions that are conducive to EHT. We also analyzed the results of three EHT indices (TXx, TX90p and HW) in two sensitivity experiments (PpAn and PnAp). Compared to PpAn, more enhanced, more frequent, and more persistent EHT events occurred in PnAp (Fig. 12). Figure 13a, g show that the summer Tmax and Z500 over NC in Ap is higher and stronger than in An. The same results are showed in Fig. 13b, h but for the Pn and Pp. These indicate that $-$ PDO or $+$ AMO can rise summer temperature in NC. Compared to the $-$ PDO (Pn), $+$ AMO (Ap) seems to be more conducive to getting warm in NC (Fig. 13c, i),

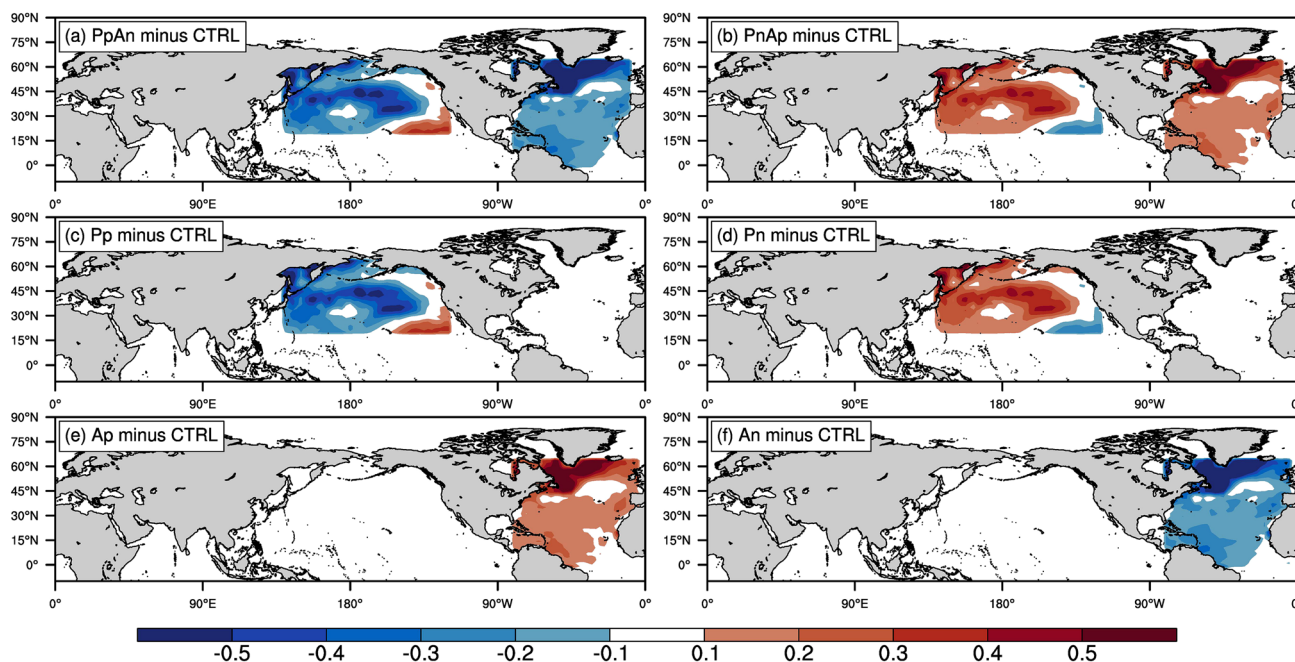


Fig. 10 Summer SSTA ($^{\circ}$ C) for **a** PnAp, **b** PpAn, **c** Pp, **d** Pn, **e** Ap and **f** An. SSTA is the input SST of each sensitive experiment minus the input SST of CTRL experiment

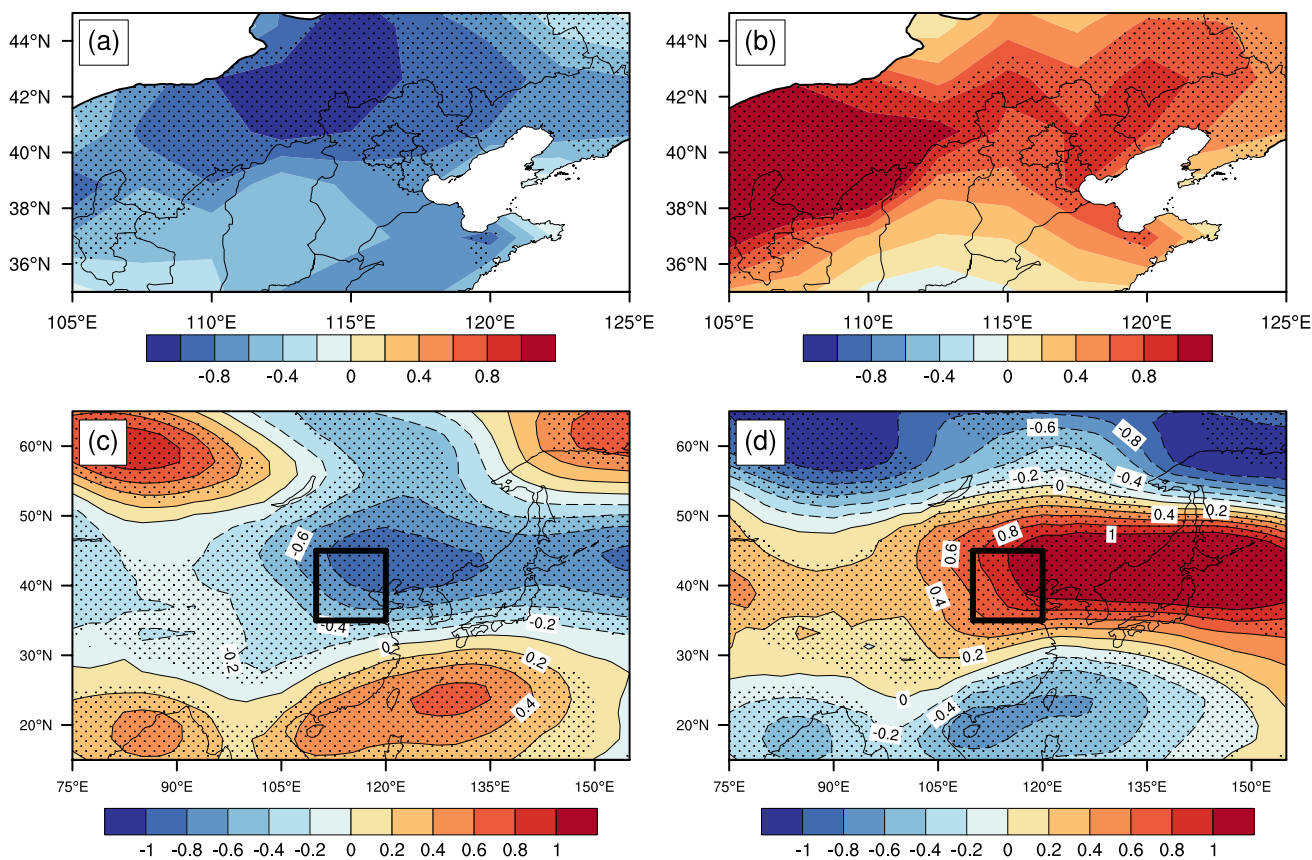


Fig. 11 Summer Tmax anomalies (shaded, °C) for PpAn (a) and PnAp (b). Geopotential height anomalies at 500 hPa (shaded, dagpm) for PpAn (c) and PnAp (d). Anomalies are PpAn/PnAp minus CTRL.

Dotted areas denote statistical significance at the 0.05 level according to the Student's *t*-test

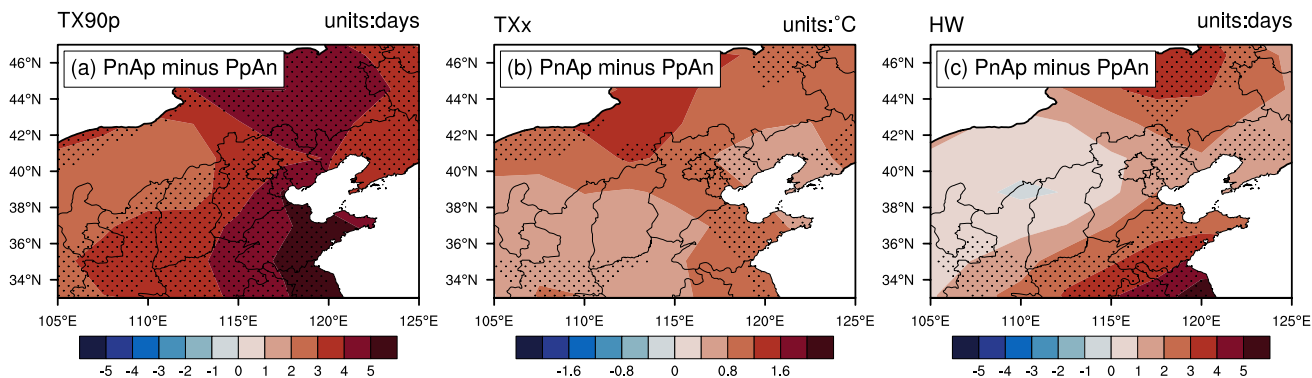


Fig. 12 Difference between PnAp and PpAn for a TX90p, b TXx and c HW. Dotted areas denote statistical significance at the 0.05 level according to the Student's *t*-test

which proves that the AMO is dominant of the impacts on NC's EHT. Figure 13d, f show that the summer Tmax of PnAp is higher than that of Ap and Pn. Thus, the combination of $-$ PDO and $+$ AMO (PnAp) also has more impacts on NC's Tmax than their individual impacts.

The clockwise/counter-clockwise vertical circulation anomalies from NC to the Sea of Japan and the CAC/ACA circulation anomalies in the upper level are both shown in the results of PpAn/PnAp (Fig. 14a, b, e, f). Besides that, the individual results of Pp/Pn are also similar: Fig. 14c, d shows that there are upward/downward motions over

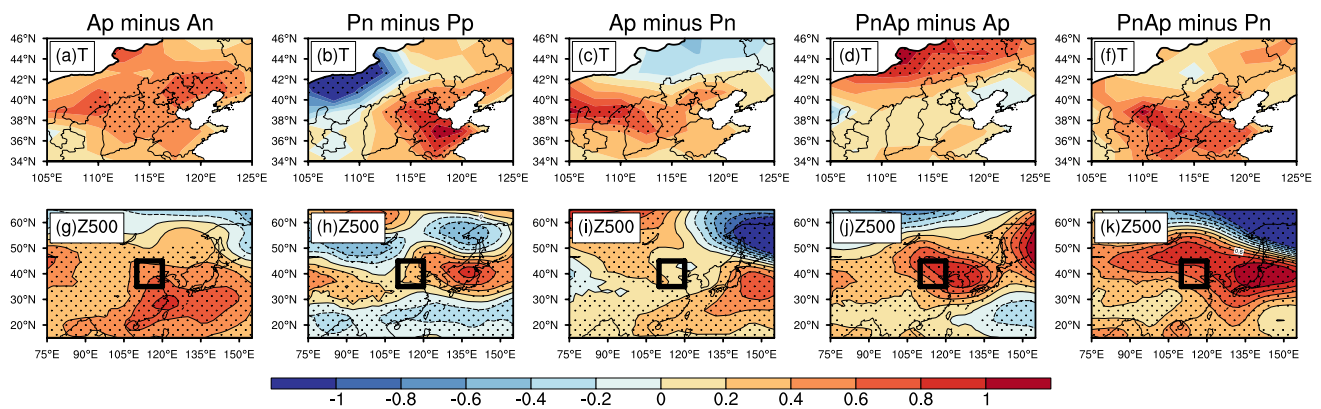


Fig. 13 a–f The summer Tmax differences (shaded, °C). g–k The same as (a)–(f), but for the geopotential height differences at 500 hPa (shaded, dagpm). (a)/(b) Is Ap minus An, (b)/(h) is Pn minus Pp, (c)/(i) is Ap minus Pn, (d)/(j) is PnAp minus Ap, and (f)/(k) is PnAp

minus Pn. The black frame in the figure shows the location of North China. Dotted areas denote statistical significance at the 0.05 level according to the Student's *t*-test

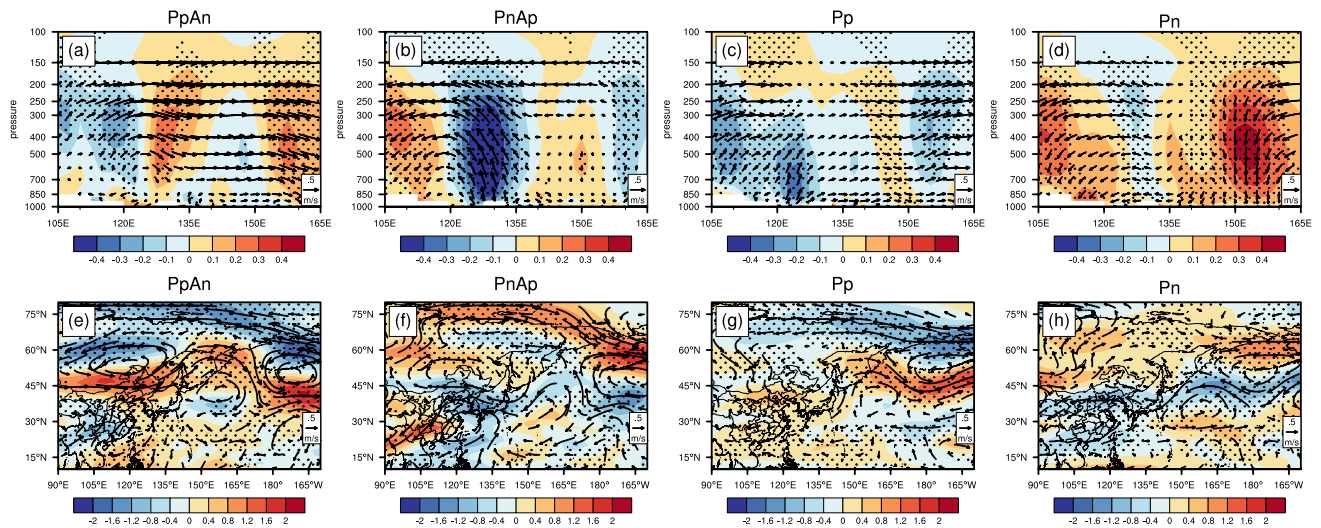


Fig. 14 Longitude-pressure sections of vertical circulation anomalies averaged from 35° to 45°N of the a PpAn, b PnAp, c An and d Ap (vector, units of vertical and meridional wind are 10⁻² Pa/S and m/s, respectively; shaded is vertical velocity). Horizontal wind anomalies

(vector, m/s, shaded is meridional velocity) at 200 hPa of the e PpAn, f PnAp, g An and h Ap. Anomalies are the simulations minus CTRL. Dotted areas denote statistical significance at the 0.05 level according to the Student's *t*-test

NC and the westerly/easterly winds in the high level; the CAC/ACA anomalies are also above the mid-latitudes (Fig. 14d, h). Therefore, the experimental results prove the mechanism of PDO's impacts on NC in the observation conclusion. In addition, the cyclonic-anticyclonic teleconnection wave trains in the midlatitudes of the Northern Hemisphere also appeared in their results (Fig. 15). Although there was little positional deviation in the peaks and troughs of the wave trains, the circulations over NP, NA and NC are very similar to the observations. Figure 16 shows the results of the geopotential height anomalies and WAF at 300 hPa. The eastward WAF of each experiment also indicates that the wave train mainly starts from the

NA and crosses the Eurasian continent in the midlatitudes to the NP. Not only the combination simulations (PpAn and PnAp, Fig. 16a, b) but also the individual simulations for AMO (An and Ap, Fig. 16c, d) are similar to the observations. In summary, the results of the numerical experiments are very similar to the observations, and prove that – PDO and + AMO are conducive to the EHT events in NC. The individual simulations show that both + AMO and – PDO can lead the EHT in NC. Compared to – PDO, + AMO lead to warmer NC, which proves that the impact of AMO on NC is dominant.

The results of the model experiments have proven the previous conclusions. The combination of – PDO and +

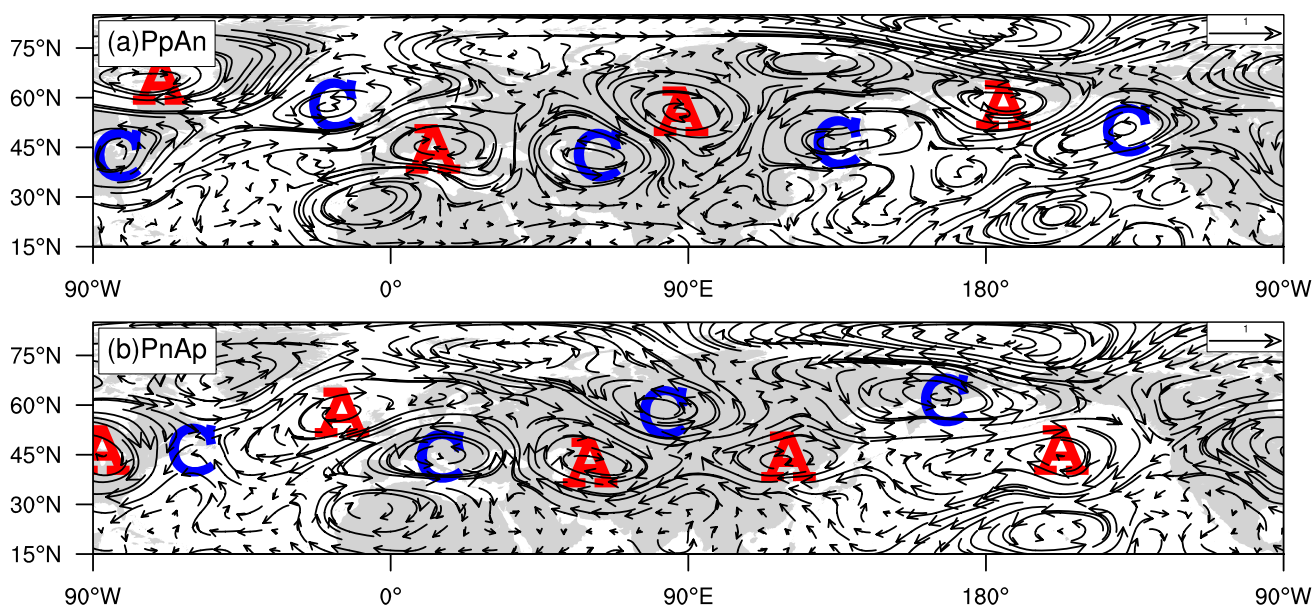


Fig. 15 Same as in Fig. 8 but for the anomalies of PpAn (a) and PnAp (b)

AMO can cause anticyclonic circulation anomalies over the NP and NA. The impact of AMO on the EHT in NC is dominant. The anticyclonic circulation anomalies over NA are the parts of the teleconnection wave train in the midlatitudes of the Northern Hemisphere. These anticyclonic circulation anomalies could affect the wave train and cause the anticyclonic circulation anomalies over NC. It could strengthen the continental high and weaken the upper zonal westerly over NC and eventually result in conditions that are favorable for the EHT. The anticyclonic circulation anomalies over NP can enhance the anticyclonic anomalies over NC through the PEA, and the ACA from NC to the NNP can also lead a counter-clockwise vertical circulation from NC to the Sea of Japan. This vertical circulation would cause the downward motion and the upper easterly wind over NC, which could weaken the upper zonal westerly. For the combination of +PDO and -AMO, the reversed atmosphere circulations would cause the cyclonic circulation anomalies and enhance the upper zonal westerly over NC.

6 Conclusions and discussion

6.1 Conclusions

Based on the CPC daily maximum air temperature datasets and three EHT indices (TX_x, TX_{90p}, HW) from 1979 to 2018, the interdecadal variation in summer EHT events in NC was analyzed. An interdecadal shift occurred in 1996 with the years before 1996 (1983–1996) being a cold period

and the following years (1997–2014) being a warm period. Comparing the differences in atmospheric circulation anomalies in the two periods, the results indicate that the increases in the continental high and weakening of the zonal westerly over NC are the main factors for EHT events in NC.

The summer SSTA distribution of the cold (heat) period shows a pattern such as + PDO (– PDO) in the NP and a pattern such as – AMO (+ AMO) in the NA. The time series of the summer PDO and AMO, which show similar interdecadal variations with NC's Tmax, where the PDO turns from positive to negative and the AMO turns from negative to positive in the mid-late 1990s, have significant negative and positive correlations with the EHT events in NC.

Further observational analysis showed that PDO and AMO could affect NC through the PEA and the cyclonic-anticyclonic teleconnection wave train in the midlatitudes of the Northern Hemisphere, respectively (Fig. 17). During the warm period (– PDO and + AMO), warmer SSTA in the NP and NA could cause anticyclonic circulation anomalies over each basin. The anticyclonic circulation anomalies over NA are parts of the wave train. These anticyclonic anomalies could influence the wave train to cause the anticyclonic circulation anomalies over NC. This would strengthen the continental high and weaken the upper zonal westerly over NC and eventually result in the EHT events in NC. The anticyclonic circulation anomalies over NP can enhance the anticyclone over NC through the PEA, and the ACA from NC to NP can also lead a counter-clockwise vertical circulation from NC to the Sea of Japan. This vertical circulation would cause the downward motion and weaken the upper zonal westerly. In the cold period (+PDO and – AMO), due

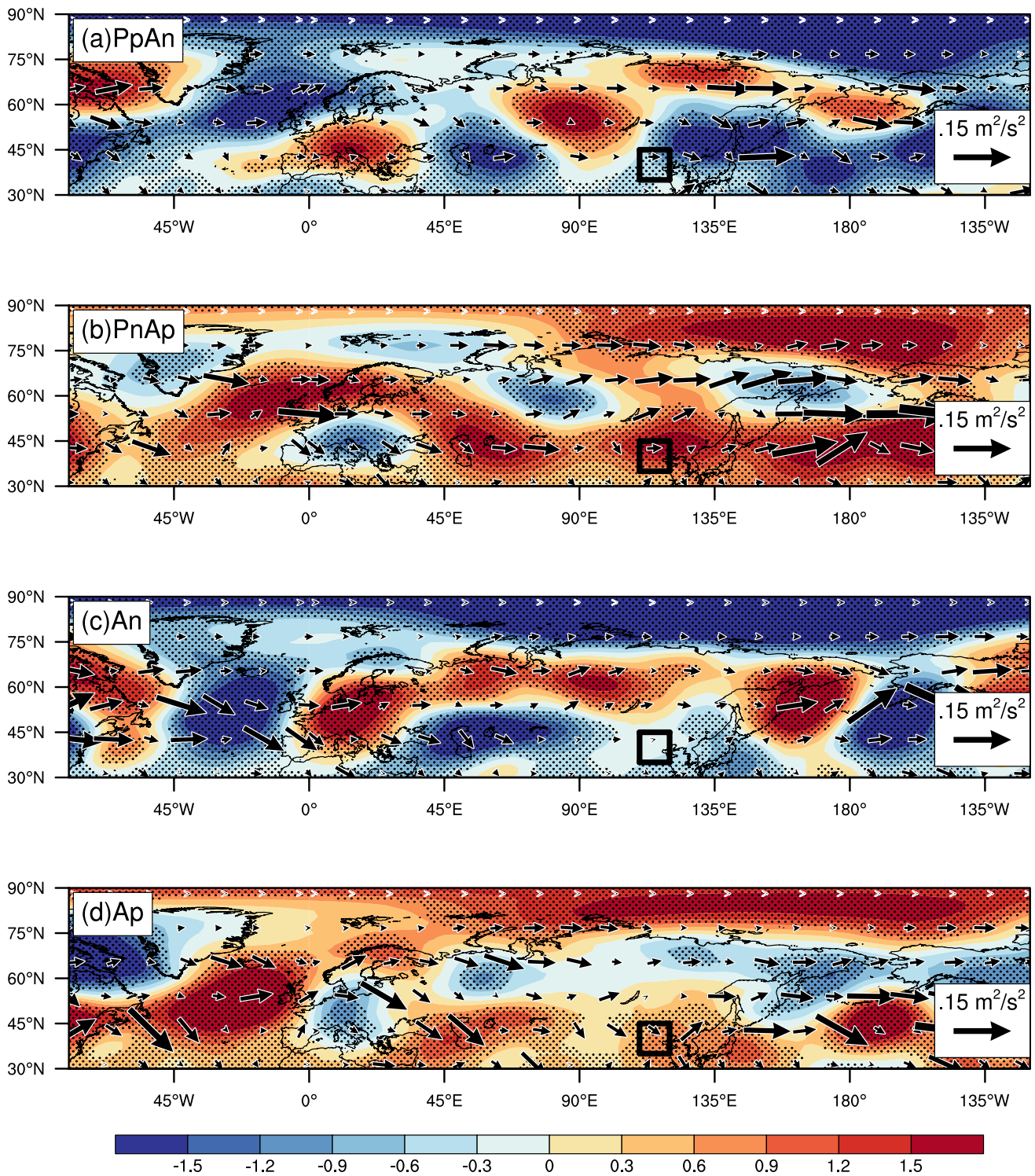


Fig. 16 Geopotential height anomalies (shading, dagpm) and WAF (vector, $m^2 \cdot s^{-2}$) at 300 hPa of the **a** PpAn, **b** PnAp, **c** An and **d** Ap. Anomalies are the simulations minus CTRL. Dotted areas denote statistical significance at the 0.05 level according to the Student's *t*-test

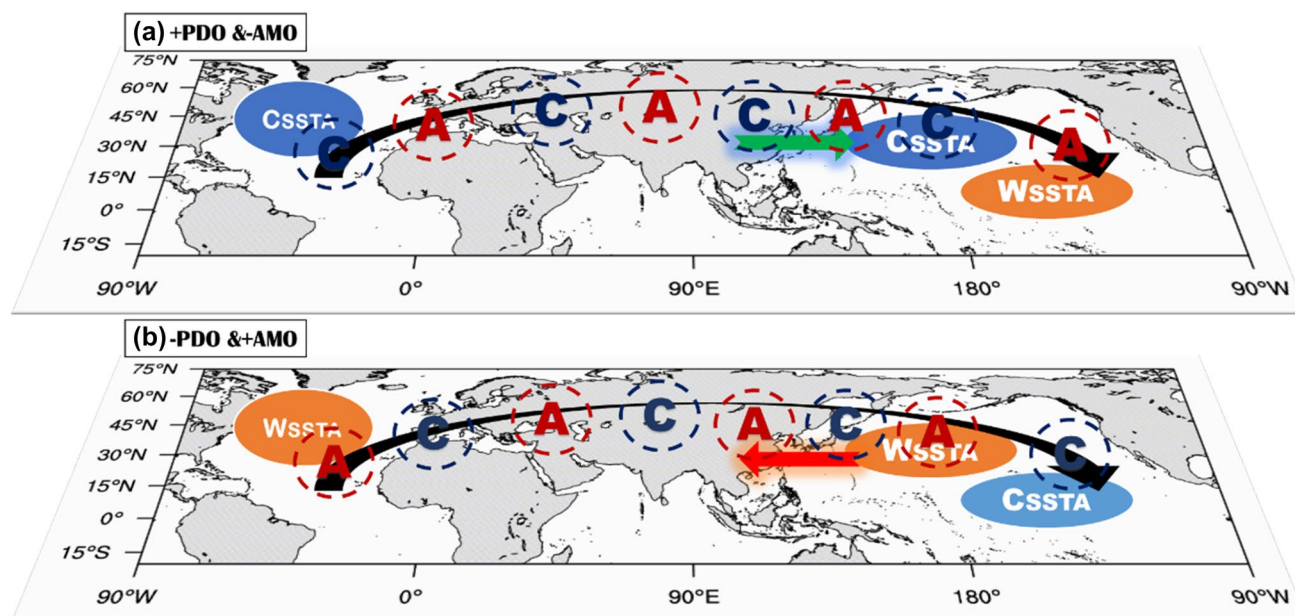


Fig. 17 Schematic diagram of the impacts of +PDO and –AMO **a** and –PDO and +AMO **b** on the interdecadal variations in North China's EHT. Red A and blue C denote an anticyclone and cyclone of the teleconnection wave train in the midlatitudes of the Northern

Hemisphere, respectively. The W_{SSTA} and C_{SSTA} denote warm and cold SSTA, respectively. The green/red straight line with an arrow represents the enhanced/weakened upper zonal westerly. The black curve with an arrow denotes the teleconnection wave trains

to the same atmospheric response mechanism, a wave train with reversed anomaly centers and the clockwise vertical circulation from NC to the Sea of Japan were also found. The cyclonic anomalies over NC are not conducive to the EHT. Therefore, the combination of +PDO and –AMO changing to –PDO and +AMO has a great impact on the interdecadal shift in EHT in NC in 1996. Both the +AMO and –PDO can lead the EHT in NC individually, and the impact of AMO is dominant.

Based on observational analysis, we carried out one control experiment and six sensitivity experiments using the CAM5.3 atmospheric model. The numerical results proved the observational analysis. The results of this study indicate that an important reason for the interdecadal transitions of the summer EHT in NC in approximately 1996 was the shift in PDO and AMO.

6.2 Discussion

The limitations of the current research should be recognized. First, only the interdecadal variation in EHT in NC during the 1979–2018 period was analyzed. Compared with this period of +AMO and –PDO, the results from Zhang et al. (2018) showed that the +AMO and –PDO during 1946–1961 had some different impacts on the ESAM. Whether the correlation between the EHT in

NC and the combination of AMO and PDO existed before 1979 needs further study. Second, future studies that use air-sea coupled models may be helpful for making a stronger correlation between the EHT in NC and the combination of AMO and PDO. Third, the effects of in-phase AMO and PDO on the EHT also require further study. This may need to be based on long-term observational data or long-term reconstruction data to obtain enough samples. In addition, AMO is dominant of the 1996's shift. What about other shifts? More analysis may be needed to find which circulations have greater contributions to the EHT in NC. Finally, similar limitations will arise in the research on interannual variations in the EHT in NC.

Acknowledgements We appreciate the Editor and three anonymous reviewers for their critical comments and suggestions which helped to improve the quality of paper. This research is supported by the National Key Research and Development Program of China (2017YFA0603804), the National Natural Science Foundation of China (41575085 and 41430528) and the Postgraduate Research and Practice Innovation Program of Jiangsu Province (KYCX19_1026).

References

Aiken LS, West SG (1991) Multiple regression: testing and interpreting interactions. Sage, Newbury Park

- Barrio P et al (2011) The hot summer of 2010: redrawing the temperature record map of Europe. *Science* 332(6026):220–224. <https://doi.org/10.1126/science.1201224>
- Bretherton CS, Widmann M, Dymnikov VP, Wallace JM, Bladé I (1999) The effective number of spatial degrees of freedom of a time-varying field. *J Clim* 12:1990–2009. <https://doi.org/10.1175/1520-0442>
- Cheng Q, Zhou TJ (2014) Multidecadal variability of north china aridity and its relationship to PDO during 1900–2010. *J Clim* 27(3):1210–1222. <https://doi.org/10.1175/jcli-d-13-00235.1>
- Delworth TL, Mann ME (2000) Observed and simulated multi-decadal variability in the Northern hemisphere. *Clim Dyn* 16:661–671. <https://doi.org/10.1007/s003820000075>
- Delworth TL, Zeng F, Vecchi GA, Yang X, Zhang L, Zhang R (2016) The North Atlantic Oscillation as a driver of rapid climate change in the Northern hemisphere. *Nat Geosci* 9:509–512. <https://doi.org/10.1038/ngeo2738>
- Deng K, Song Y, Ting M, Lin A, Wang Z (2018) An intensified mode of variability modulating the summer heat waves in eastern Europe and northern China. *Geol Res Lett* 45(11):361–369. <https://doi.org/10.1029/2018GL079836>
- Deng K, Song Y, Lin A, Li C, Hu C (2019) Unprecedented East Asian warming in spring 2018 linked to the North Atlantic tripole SST mode. *Atmos Ocean Sci Lett* 12(4):246–253. <https://doi.org/10.1080/16742834.2019.1605807>
- Ding T, Qian WH, Yan SW (2009) Changes in hot days and heat waves in China during 1961–2007. *Int J Climatol* 30:1452–1462. <https://doi.org/10.1002/joc.1989>
- Duchon CE (1979) Lanczos filtering in one and two dimensions. *J Appl Meteorol* 18(8):1016–1022. [https://doi.org/10.1175/1520-0450\(1979\)018%3c1016:LFOAT%3e2.0.CO;2](https://doi.org/10.1175/1520-0450(1979)018%3c1016:LFOAT%3e2.0.CO;2)
- Fischer EM, Knutti R (2015) Anthropogenic contribution to global occurrence of heavy-precipitation and high-temperature extremes. *Nat Clim Chang* 5(6):560–564. <https://doi.org/10.1038/nclim.ate2617>
- Ghosh R, Müller WA, Baehr J, Bader J (2017) Impact of observed North Atlantic multidecadal variations to European summer climate: a linear baroclinic response to surface heating. *Clim Dyn* 48:3547–3563. <https://doi.org/10.1007/s00382-016-3283-4>
- Gong DY, Ho CH (2003) Arctic Oscillation signals in the East Asian summer monsoon. *J Geophys Res* 108:4066. <https://doi.org/10.1029/2002JD002193>
- Gulev SK et al (2013) North Atlantic Ocean-control on surface heat flux on multidecadal timescales. *Nature* 499(7459):464–467. <https://doi.org/10.1038/nature12268>
- Han T, He S, Xin H, Wang H (2017) Recent interdecadal shift in the relationship between Northeast China's winter precipitation and the North Atlantic and Indian Oceans. *Clim Dyn* 50(3–4):1413–1424. <https://doi.org/10.1007/s00382-017-3694-x>
- Huang DQ, Dai AG, Yang B, Yan P, Zhu J, Zhang YC (2018) Contributions of different combinations of the IPO and AMO to recent changes in winter East Asian Jets. *J Clim*. <https://doi.org/10.1175/jcli-d-18-0218.1>
- Kanamitsu M, Ebisuzaki W, Woollen J, Yang SK, Hnilo JJ, Fiorino M, Potter GL (2002) NCEP-DOE AMIP-II reanalysis (R-2). *Bull Am Meteorol Soc*. <https://doi.org/10.1175/BAMS-83-11-1631>
- Kucharski F, Bracco A, Yoo JH, Tompkins AM, Feudale L, Rutti P, Dell'Aquila A (2009) A Gill-Matsuno-type mechanism explains the tropical Atlantic influence on African and Indian monsoon rainfall. *Q J R Meteorol Soc* 135(640):569–579. <https://doi.org/10.1002/qj.406>
- Lei YN, Gong DY, Zhang ZY, Guo D, He XZ (2009) Spatial-temporal characteristics of high-temperature events in summer in eastern China and the associated atmospheric circulation. *Geograph Res* 28(3):654–662 (in Chinese)
- Li S, Bates GT (2007) Influence of the Atlantic multidecadal oscillation on the winter climate of East China. *Adv Atmos Sci* 24(1):126–135. <https://doi.org/10.1007/s00376-007-0126-6>
- Li RX, Sun JQ (2017) Interdecadal variability of the large-scale extreme hot event frequency over the middle and lower reaches of the Yangtze River basin and its related atmospheric patterns. *Atmos Ocean Sci Lett* 11(1):63–70. <https://doi.org/10.1080/16742834.2017.1335580>
- Liang XZ, Wang WC (1998) Association between China monsoon rainfall and tropospheric jets. *Q J R Meteorol Soc* 124:2597–2623
- Lu RY, Oh JH, Kim BJ, Beak HJ, Huang RH (2001) Associations with the interannual variations of onset and withdrawal of the Changma. *Adv Atmos Sci* 18(6):1066–1080. <https://doi.org/10.1002/qj.49712455204>
- Mantua NJ, Hare SR, Zhang Y, Wallace JM, Francis RC (1997) A Pacific Interdecadal Climate Oscillation with impacts on Salmon production. *Bull Am Meteorol Soc* 78(6):1069–1079. <https://doi.org/10.1175/1520-0477>
- McGregor GR, Ferro CAT, Stephenson DB (2005) Projected changes in extreme weather and climate events in Europe. Extreme weather events and public health responses. Springer, Berlin. https://doi.org/10.1007/3-540-28862-7_2
- Meehl GA, Tebaldi C (2004) More intense, more frequent, and longer lasting heat waves in the 21st century. *Science* 305(5686):994–997. <https://doi.org/10.1126/science.1098704>
- Miao JP, Wang T, Wang HJ (2019) Interdecadal variations of the East Asian winter monsoon in CMIP5 preindustrial simulations. *J Clim*. <https://doi.org/10.1175/JCLI-D-19-0148.1>
- Napoli A, Crespi A, Ragone F, Maugeri M, Pasquero C (2019) Variability of orographic enhancement of precipitation in the Alpine region. *Sci Rep* 9(1). <https://doi.org/10.1038/s41598-019-49974-5>
- Neale RB et al (2012) Description of the NCAR community atmosphere model (CAM5.0). NCAR Tech Note NCAR/TN-486 +STR, p 274
- Plumb RA (1985) On the three-dimensional propagation of stationary waves. *J Atmos Sci* 42(3):217–229. [https://doi.org/10.1175/1520-0469\(1985\)042%3c0217:OTDPO%3e2.0.CO;2](https://doi.org/10.1175/1520-0469(1985)042%3c0217:OTDPO%3e2.0.CO;2)
- Rayner NA, Parker DE, Horton EB, Folland CK, Alexander LV, Rowell DP, Kent EC, Kaplan A (2003) Global analyses of sea surface temperature, sea ice, and night marine air temperature since the late nineteenth century. *J Geophys Res* 108:D14. <https://doi.org/10.1029/2002jd002670>
- Si D, Ding Y (2016) Oceanic forcings of the interdecadal variability in East Asian summer rainfall. *J Clim* 29(21):7633–7649. <https://doi.org/10.1175/jcli-d-15-0792.1>
- Sun JQ (2012) Possible impact of the summer North Atlantic oscillation on extreme hot events in China. *Atmos Ocean Sci Lett* 5(3):231–234. <https://doi.org/10.1080/16742834.2012.11446996>
- Sun JQ (2014) Record-breaking SST over mid-North Atlantic and extreme high temperature over the Jianghuai–Jiangnan region of China in 2013. *Chin Sci Bull* 59:3465–3470. <https://doi.org/10.1007/s11434-014-0425-0> (in Chinese)
- Sun JQ, Wang HJ, Yuan W (2008) Decadal variations of the relationship between the summer North Atlantic Oscillation and middle East Asian air temperature. *J Geophys Res* 113:D15107. <https://doi.org/10.1029/2007JD009626>
- Sun JQ, Wang HJ, Yuan W (2011) Decadal variability of the extreme hot events in China and its associated with atmospheric circulations. *Clim Environ Res* 16(2):199–208 (in Chinese)
- Tao P, Zhang Y (2019) Large-scale circulation features associated with the heat wave over Northeast China in summer 2018. *Atmos Ocean Sci Lett* 12(4):254–260. <https://doi.org/10.1080/16742834.2019.1610326>
- Trednberth KE, Shea DJ (2006) Atlantic hurricanes and natural variability in 2005. *Geol Res Lett* 33(12):L12704. <https://doi.org/10.1029/2006gl026894>

- Wang Y, Li S, Luo D (2009) Seasonal response of Asian monsoonal climate to the Atlantic Multidecadal Oscillation. *J Geophys Res* 114:D02112. <https://doi.org/10.1029/2008JD010929>
- Wang YJ, Ren FM, Zhang XB (2013) Spatial and temporal variations of regional high temperature events in China. *Int J Clim* 34(10):3054–3065. <https://doi.org/10.1002/joc.3893>
- Wang L, Xu P, Chen W, Liu Y (2017) Interdecadal variations of the silk road pattern. *J Clim* 30(24):9915–9932. <https://doi.org/10.1175/jcli-d-17-0340.1>
- Wang M, Gu Q, Jia X, Ge J (2019) An assessment of the impact of PDO on autumn droughts in North China based on the PDSI. *Int J Clim* 39:5338–5350. <https://doi.org/10.1002/joc.6158>
- Wei J, Yang H, Sun SQ (2004) Relationship between the anomaly longitude position of subtropical high in the western Pacific and severe hot weather in North China in summer. *Acta Meteorol Sin* 62(3):308–316 (in Chinese)
- Wu J, Gao XJ (2013) A gridded daily observation dataset over China region and comparison with the other datasets. *Chin J Geophys* 56:1102–1111. <https://doi.org/10.6038/cjg20130406> (in Chinese)
- Wu B, Lin J, Zhou T (2016a) Interdecadal circumglobal teleconnection pattern during boreal summer. *Atmos Sci Lett* 17:446–452. <https://doi.org/10.1002/asl.677>
- Wu B, Zhou T, Li T (2016b) Impacts of the Pacific–Japan and circumglobal teleconnection patterns on the interdecadal variability of the East Asian Summer monsoon. *J Clim* 29(9):3253–3271. <https://doi.org/10.1175/jcli-d-15-0105.1>
- Xiao D, Li J (2007) Spatial and temporal characteristics of the decadal abrupt changes of global atmosphere–ocean system in the 1970s. *J Geophys Res*. <https://doi.org/10.1029/2007jd008956>
- Xie P, Arkin PA (1997) Global precipitation: a 17-year monthly analysis based on gauge observations, satellite estimates, and numerical model outputs. *Bull Am Meteorol Soc* 78(11):2539–2558. <https://doi.org/10.1175/1520-0477>
- Xu Y, Gao XJ, Shen Y, Xu CH, Shi Y, Giorgi F (2009) A daily temperature dataset over China and its application in validating a RCM simulation. *Adv Atmos Sci* 26:763–772. <https://doi.org/10.1007/s00376-009-9029-z>
- Yang H, Li CY (2005) Diagnostic study of serious high temperature over South China in 2003 summer. *Clim Environ Res* 10(1):80–85 (in Chinese)
- Yuan W, Sun JQ (2009) Enhancement of the summer North Atlantic Oscillation influence on Northern Hemisphere air temperature. *Adv Atmos Sci* 26(6):1209–1214. <https://doi.org/10.1007/s00376-009-8148-x>
- Zhai PM et al (1999) Changes of climate extremes in China. *Clim Chang* 42(1):203–218. <https://doi.org/10.1023/a:1005428602279>
- Zhang R, Delworth TL (2005) Simulated tropical response to a substantial weakening of the Atlantic thermohaline circulation. *J Clim* 18:1853–1860. <https://doi.org/10.1175/JCLI3460.1>
- Zhang L, Delworth TL (2015) Analysis of the characteristics and mechanisms of the Pacific decadal oscillation in a suite of coupled models from the Geophysical Fluid Dynamics Laboratory. *J Clim* 28:7678–7701. <https://doi.org/10.1175/JCLI-D-14-00647.1>
- Zhang Y, Wallace JM, Battisti DS (1997) ENSO-like interdecadal variability: 1900–1993. *J Clim* 10(5):1004–1020. <https://doi.org/10.1175/1520-0442>
- Zhang GW, Zeng G, Ni DH, Zhou GB (2016) Decadal shift of autumn drought in Southwest China and its possible causes. *Chin J Atmos Sci* 40(2):311–323. <https://doi.org/10.3878/j.issn.1006-9895.1503.14294> (in Chinese)
- Zhang ZQ, Sun XG, Yang XQ (2018) Understanding the interdecadal variability of East Asian summer monsoon precipitation: joint influence of three oceanic signals. *J Clim* 31(14):5485–5560. <https://doi.org/10.1175/JCLI-D-17-0657.1>
- Zhu J, Huang DQ, Zhang YC, Huang AN, Kuang XY, Huang Y (2013) Decadal changes of meiyu rainfall around 1991 and its relationship with two types of ENSO. *J Geophys Res Atmos* 118:9766–9777. <https://doi.org/10.1002/jgrd.50779>
- Zhu YL, Wang T, Ma JH (2016) Influence of internal decadal variability on the summer rainfall in eastern China as simulated by CCSM4. *Adv Atmos Sci* 33(6):706–714. <https://doi.org/10.1007/s00376-016-5269-x>

Publisher's Note Springer Nature remains neutral with regard to jurisdictional claims in published maps and institutional affiliations.